Composites Engineering, Vol. 2, No 8, pp. 641–654, 1992.
Author prepared reprint
0961-9526/92 $5.00+ .00

VARIATIONAL MECHANICS ANALYSIS OF STRESSES AND FAILURE IN MICRODROP DEBOND SPECIMENS

ROBERT J. SCHEER and JOHN A. NAIRN
Department of Material Science and Engineering, University of Utah, Salt Lake City, UT 84112, U.S.A.

(*Received 26 August 1991; final version accepted 30 January 1992*)

Abstract—A recently derived variational mechanics analysis of stresses in embedded single fibers has been applied to the analysis of the stresses in the microdrop debond specimen. The new analysis is more accurate than the commonly applied shear-lag or elastic-plastic analyses. The results from a sample stress state calculation suggest that interfacial failure between the fiber and the microdrop may be by mode I or opening mode failure at the beginning of the microdrop. The opening mode failure is caused by a large tensile radial stress at the fiber/matrix interface. Previous analyses of microdrop debond data have been in terms of an average shear stress. We suggest that these analyses misrepresent microdrop debond results and recommend alternative failure analyses using energy release rate, average energy, or maximum stress. The energy failure analyses can be used to define an interfacial fracture toughness.

INTRODUCTION

To study the fiber/matrix interface, many researchers rely on single-fiber model composite tests. These tests include single-fiber fragmentation tests (Wadsworth and Spilling, 1968; Frasier *et al.*, 1975, 1983; Drzal *et al.*, 1980, 1982, 1983, 1985; Rich and Drzal, 1986; Bascom and Jensen, 1986; Folkes and Wong, 1987; DiLandro and Pegoraro, 1986; DiLandro *et al.*, 1988; DiBenedetto and Lex, 1989; Netravali *et al.*, 1989), fiber pull-out tests (Piggott *et al.*, 1985, Piggott, 1987, Penn *et al.*, 1983), microindentation tests (Mandell *et al.*, 1980), and microdrop debond tests (Gaur and Miller, 1989). The results of these various tests are significant, but the quantitative interpretation of the results has been limited by the near universal use of simplistic stress analyses such as shear-lag models (Cox, 1952, Rosen, 1964, Amirbayat and Hearle, 1969) or elastic-plastic analyses (Kelly and Tyson, 1965). A recent paper by Nairn (1992) describes a new approach to the analysis of stresses in embedded single fibers. The new analysis uses variational mechanics, achieves a closed-form solution, and is more accurate than previous analyses. In this paper we apply the variational mechanics analysis to the specific analysis of stresses in a microdrop debond specimen. A precursor to this paper appeared in Scheer and Nairn (1991). This latter reference, however, was based on a preliminary version of Nairn (1992) that contained a less accurate variational mechanics analysis. This paper replaces Scheer and Nairn (1991) by using the final, accurate variational mechanics analysis in Nairn (1992). This paper also contains new detail about microdrop specimen failure analysis.

The geometry for the analysis of stresses in embedded single fibers is shown in Fig. 1. The fiber is embedded in a cylinder of matrix. The interface between the fiber and matrix is assumed to be intact. The stress analysis thus applies up to the point of interfacial failure. The stress state at the time of interfacial failure will give us information about the level of fiber-matrix adhesion. In other words, although the stress analysis does not explicitly include an imperfect interface or interphase, the stress solution can be useful for interpreting experiments aimed at measuring the fiber-matrix adhesion. The stresses in the embedded single fiber specimen (see Fig. 1) are axisymmetric. The presence of breaks or discontinuities in the fiber or matrix does not disturb the axial symmetry. The analysis in Nairn (1992) makes only one assumption. It assumes σ_{zz} within each cylinder (fiber or matrix) depends only on the z coordinate and is independent of the r coordinate. A general stress state for a transversely isotropic fiber in an isotropic matrix that satisfies the one assumption as well

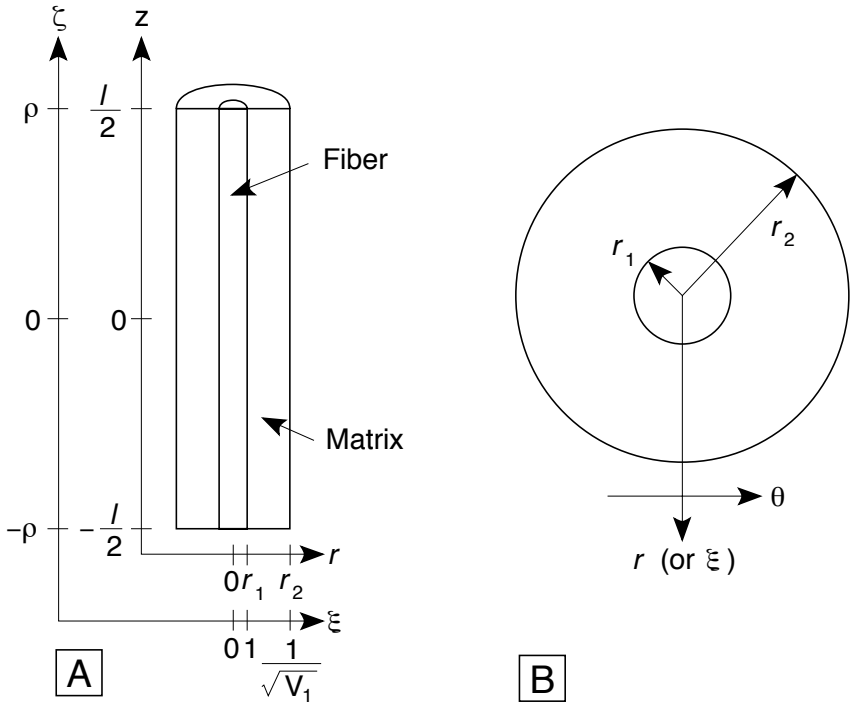

Fig. 1. The two-cylinder model used for the axisymmetric stress analysis. A single fragment of length l showing the axial and radial coordinates in both dimensioned and dimensionless forms. B: A cross-section of the two- cylinder model showing the fiber of radius r_1 and the matrix of radius r_2.

as stress equilibrium, traction boundary conditions, and some compatibility conditions is quoted from Nairn (1992). The stresses in the fiber are:

$$\sigma_{zz,1} = \psi \tag{1}$$

$$\tau_{rz,1} = -\frac{\xi\psi'}{2} \tag{2}$$

$$\sigma_{rr,1} = \frac{\psi''}{16}\left(\xi^2(3+\nu_T)+\nu_m-\nu_T+\frac{2(1+\nu_m)\ln V_1}{V_2}-\frac{V_2A_1}{V_1A_0}\right) - \frac{V_2}{V_1}\left(\frac{A_3\psi+A_4\sigma_0+A_5\Delta T}{A_0}\right) \tag{3}$$

$$\sigma_{\theta\theta,1} = \frac{\psi''}{16}\left(\xi^2(1+3\nu_T)+\nu_m-\nu_T+\frac{2(1+\nu_m)\ln V_1}{V_2}-\frac{V_2A_1}{V_1A_0}\right) - \frac{V_2}{V_1}\left(\frac{A_3\psi+A_4\sigma_0+A_5\Delta T}{A_0}\right). \tag{4}$$

The stresses in the matrix are:

$$\sigma_{zz,2} = \frac{\sigma_0}{V_2}-\frac{V_1\psi}{V_2} \tag{5}$$

$$\tau_{rz,2} = \frac{V_1\psi'}{2V_2}\left(\xi-\frac{1}{\xi V_1}\right) \tag{6}$$

$$\sigma_{rr,2} = \frac{\psi''}{16V_2}\left[(3+\nu_m)\left(1-\xi^2V_1\right)+2(1+\nu_m)\ln\xi^2V_1+\frac{V_2A_1}{A_0}\left(1-\frac{1}{\xi^2V_1}\right)\right] + \left(1-\frac{1}{\xi^2V_1}\right)\left(\frac{A_3\psi+A_4\sigma_0+A_5\Delta T}{A_0}\right) \tag{7}$$

$$\sigma_{\theta\theta,2} = \frac{\psi''}{16V_2}\left[(1+3\nu_m)\left(1-\xi^2V_1\right)-2(1-\nu_m)+2(1+\nu_m)\ln\xi^2V_1+\frac{V_2A_1}{A_0}\left(1+\frac{1}{\xi^2V_1}\right)\right]$$

$$+\left(1+\frac{1}{\xi^2 V_1}\right)\left(\frac{A_3\psi + A_4\sigma_0 + A_5\Delta T}{A_0}\right) \tag{8}$$

where V_1 and V_2 are the volume fractions of the fiber and the matrix, ν_T is the transverse Poisson's ratio of the fiber, ν_m is the Poisson's ratio of the matrix, A_0 to A_5 are constants defined in the Appendix, σ_0 is the total axial stress applied in the z direction, $\Delta T = T_s - T_0$ is the temperature difference between the specimen temperature (T_s) and the stress-free temperature (T_0), ξ is a dimensionless radial coordinate defined by $\xi = r/r_1$, and the applied radial stress is zero. The stresses are defined in terms of a single unknown function $\psi(\zeta)$, where ζ is a dimensionless axial coordinate defined by $\zeta = z/r_1$. By axial symmetry, the unspecified shear stresses are all zero.

The stresses in eqns (1)–(8) constitute an admissible stress state. By the principles of variational mechanics, the best approximation to the true stress state is found by finding the $\psi(\zeta)$ that minimizes the total complementary energy. In Nairn (1992), a calculus of variations approach was used to derive a fourth order differential equation for $\psi(\zeta)$:

$$\psi^{iv} + p\psi'' + q\psi = q\psi_0 \tag{9}$$

where ψ_0 is a constant defined by (Nairn, 1992):

$$\psi_0 = -\frac{C_{13}\sigma_0 + D_3\Delta T}{C_{33}}. \tag{10}$$

C_{ij}, D_i, p, and q are constants that are defined in the Appendix. We can write the solution to eqn (9) as

$$\psi(\zeta) = \psi_0 - \phi(\zeta) \tag{11}$$

where $\phi(\zeta)$ is the solution to the homogeneous, fourth-order differential equation

$$\phi^{iv} + p\phi'' + q\phi = 0. \tag{12}$$

MICRODROP SPECIMEN ANALYSIS

A typical microdrop debond specimen with a microdrop of length l and aspect ratio ρ ($\rho = l/2r_1$) is shown in Fig. 2A. Microdrops are nearly elliptical. A meniscus may form where the fiber enters

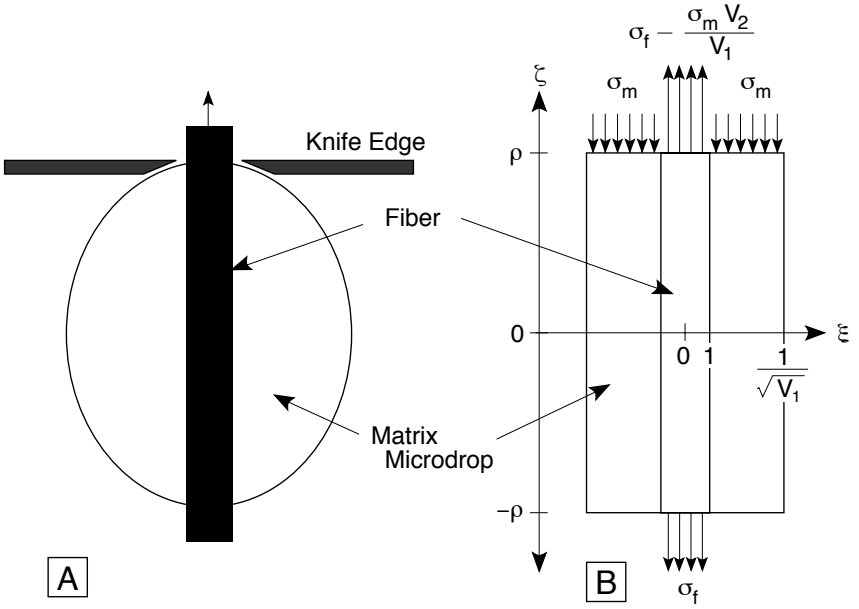

Fig. 2. A matrix microdrop of dimensionless length 2ρ. A: The microdrop specimen. B: An idealized microdrop specimen showing the boundary conditions relevant to the microdrop debond test. σ_f is the background fiber tensile stress. σ_m is the stress applied to the microdrop during the test.

the microdrop. Observations, however, show that a typical meniscus is small and does not significantly distort the elliptical shape (Gaur and Miller, 1989). In the typical experiment, a fiber with a microdrop is loaded into a tensile testing jig. A small amount of fiber load may be used to achieve fiber alignment. A pair of knife edges contact the matrix microdrop near the fiber and the fiber is pulled until the interface fails (Gaur and Miller, 1989).

We idealize the microdrop specimen by replacing the microdrop with a cylinder and by replacing the knife edge loading with uniform axisymmetric loading. The length of the cylinder is chosen to match the length of the microdrop. The radius of the cylinder is chosen to preserve the effective volume fraction of the fiber within the microdrop. The initial fiber alignment load or background load is σ_f. This load is typically small and may be negligible. The reactive compressive load on the matrix, σ_m, that results from pulling on the fiber is distributed as a uniform stress over the top of the matrix cylinder. The compressive load on the matrix balances the pulling force and thus the total applied axial stress remains constant and is $\sigma_0 = V_1\sigma_f$. If the alignment load is negligible the total applied stress is approximately zero. Our analysis is in terms of dimensionless coordinates. The dimensionless coordinates for the idealized microdrop specimen are shown in Fig. 2B.

From Fig. 2B, the idealized microdrop debond test boundary conditions are

$$\begin{aligned} &\psi(\rho) = \sigma_f - \frac{\sigma_m V_2}{V_1} && \psi(-\rho) = \sigma_f && \psi'(\pm\rho) = 0 \\ &\phi(\rho) = \psi_0 - \frac{\sigma_0 - \sigma_m V_2}{V_1} && \phi(-\rho) = \psi_0 - \frac{\sigma_0}{V_1} && \phi'(\pm\rho) = 0. \end{aligned} \tag{13}$$

Using these boundary conditions, there are two solutions to eqn (12) depending on the roots to the characteristic equation. We express both solutions as

$$\phi(\zeta) = \left(\psi_0 - \frac{\sigma_0}{V_1} + \frac{\sigma_m V_2}{2V_1}\right)\phi_e(\zeta) + \left(\frac{\sigma_m V_2}{2V_1}\right)\phi_o(\zeta) \tag{14}$$

where $\phi_e(\zeta)$ and $\phi_o(\zeta)$ are even and odd functions of ζ. When $p^2 - 4q < 0$

$$\phi_e(\zeta) = \frac{2h_2'(\rho)\cosh\alpha\zeta\cos\beta\zeta - 2h_1'(\rho)\sinh\alpha\zeta\sin\beta\zeta}{\beta\sinh 2\alpha\rho + \alpha\sin 2\beta\rho} \tag{15}$$

$$\phi_o(\zeta) = \frac{2h_4'(\rho)\sinh\alpha\zeta\cos\beta\zeta - 2h_3'(\rho)\cosh\alpha\zeta\sin\beta\zeta}{\beta\sinh 2\alpha\rho - \alpha\sin 2\beta\rho} \tag{16}$$

where

$$\begin{aligned} &h_1(\rho) = \cosh\alpha\rho\cos\beta\rho && h_3(\rho) = \sinh\alpha\rho\cos\beta\rho && \alpha = \frac{1}{2}\sqrt{2\sqrt{q} - p} \\ &h_2(\rho) = \sinh\alpha\rho\sin\beta\rho && h_4(\rho) = \cosh\alpha\rho\sin\beta\rho && \beta = \frac{1}{2}\sqrt{2\sqrt{q} + p} \end{aligned} \tag{17}$$

and $h_i'(\rho)$ is the derivative of $h_i(\rho)$ with respect to ρ. When $p^2 - 4q > 0$

$$\begin{aligned} \phi_e(\zeta) &= \frac{\beta\cosh\alpha\zeta\operatorname{csch}\alpha\rho - \alpha\cosh\beta\zeta\operatorname{csch}\beta\rho}{\beta\coth\alpha\rho - \alpha\coth\beta\rho} \\ \phi_o(\zeta) &= \frac{\beta\sinh\alpha\zeta\operatorname{sech}\alpha\rho - \alpha\sinh\beta\zeta\operatorname{sech}\beta\rho}{\beta\tanh\alpha\rho - \alpha\tanh\beta\rho} \end{aligned} \tag{18}$$

where

$$\alpha = \sqrt{-\frac{p}{2} + \sqrt{\frac{p^2}{4} - q}} \qquad \beta = \sqrt{-\frac{p}{2} - \sqrt{\frac{p^2}{4} - q}}. \tag{19}$$

As shown in Nairn (1992), the constant ψ_0 defines the stress state far from the sample ends. In other words, setting $\psi(\zeta) = \psi_0$ and substituting in eqns (1)–(8) gives the stresses in two infinitely long concentric cylinders. Because the one assumption of σ_{zz} being independent of r is correct for infinitely long cylinders, the resulting stress state is exact. By eqn (11), we see that $\phi(\zeta)$ defines a perturbation stress or the change in stress due to finite size microdrops. $\phi(\zeta)$ will be largest near

the ends of the microdrop and approach zero far from the ends. If the microdrop is not very long, however, $\phi(\zeta)$ will not reach zero before encroaching on the opposite end of the microdrop.

For possible energy release rate calculations it is useful to calculate the total strain energy in the microdrop specimen. The total strain energy is

$$U = \frac{1}{2}\int_V \vec{\sigma}\cdot\mathbf{K}\vec{\sigma}dV \tag{20}$$

where $\vec{\sigma}$ is the stress tensor and $\mathbf{K}$ is the compliance tensor. The integration is identical to the evaluation of the complementary energy in Nairn (1992) except that some terms are dropped. The result in terms of ψ is

$$\begin{aligned} U &= \pi r_1^3\Bigg[2\rho C_{11}\sigma_0^2 + \int_{-\rho}^{\rho} d\zeta\big(C_{33}\psi^2 + 2C_{35}\psi\psi'' + C_{55}\psi''^2 \\ &\qquad + C_{44}\psi'^2 + 2C_{13}\sigma_0\psi + 2C_{15}\sigma_0\psi''\big)\Bigg] \end{aligned} \tag{21}$$

where C_{ij} are constants that are defined in the Appendix. Because of the zero shear-stress boundary conditions on the microdrop ends

$$\int_{-\rho}^{\rho}\psi''d\zeta = 0. \tag{22}$$

Integrating eqn (9) from $-\rho$ to ρ we quickly achieve

$$\int_{-\rho}^{\rho}\psi d\zeta = 2\rho\left[\psi_0 + \frac{C_{55}}{C_{33}}\left(\frac{\sigma_0}{V_1} - \frac{\sigma_m V_2}{2V_1} - \psi_0\right)\frac{\chi_e(\rho)}{\rho}\right] \tag{23}$$

where we have defined a new function $\chi_e(\rho) = -\phi_e'''(\rho)$. Following Hashin (1985) we multiply eqn (9) by $C_{33}\psi$ and integrate from $-\rho$ to ρ. After integration by parts we quickly achieve

$$\begin{aligned} &\int_{-\rho}^{\rho} d\zeta\big(C_{33}\psi^2 + 2C_{35}\psi\psi'' + C_{55}\psi''^2 + C_{44}\psi'^2\big) \\ &\qquad = 2\rho\left\{C_{33}\psi_o^2 + C_{55}\left[\left(\frac{\sigma_0}{V_1} - \frac{\sigma_m V_2}{2V_1}\right)^2 - \psi_0^2\right]\frac{\chi_e(\rho)}{\rho} + C_{55}\left(\frac{\sigma_m V_2}{2V_1}\right)^2\frac{\chi_o(\rho)}{\rho}\right\} \end{aligned} \tag{24}$$

where we have defined a new function $\chi_o(\rho) = -\phi_o'''(\rho)$. Combining eqns (21)–(24), a closed-form expression for the total strain energy is

$$\begin{aligned} U &= 2\rho\pi r_1^3\Bigg\{C_{11}\sigma_0^2 + C_{33}\psi_0^2 + 2C_{13}\sigma_0\psi_0 + \frac{C_{55}\chi_0(\rho)}{\rho}\left(\frac{\sigma_m V_2}{2V_1}\right)^2 \\ &\qquad + \frac{C_{55}\chi_e(\rho)}{\rho}\left[\left(\left(\frac{\sigma_0}{V_1} - \frac{\sigma_m V_2}{2V_1}\right)^2 - \psi_0^2\right) + \frac{2C_{13}\sigma_0}{C_{33}}\left(\frac{\sigma_0}{V_1} - \frac{\sigma_m V_2}{2V_1} - \psi_0\right)\right]\Bigg\}. \end{aligned} \tag{25}$$

The two new functions, $\chi_e(\rho)$ and $\chi_0(\rho)$, have the following explicit forms. When $p^2 - 4q < 0$

$$\chi_e(\rho) = 2\alpha\beta\big(\alpha^2+\beta^2\big)\frac{\cosh 2\alpha\rho - cos2\beta\rho}{\beta\sinh 2\alpha\rho + \alpha\sin 2\beta\rho} \tag{26}$$

$$\chi_o(\rho) = 2\alpha\beta\big(\alpha^2+\beta^2\big)\frac{\cosh 2\alpha\rho + cos2\beta\rho}{\beta\sinh 2\alpha\rho - \alpha\sin 2\beta\rho}. \tag{27}$$

When $p^2 - 4q > 0$

$$\chi_e(\rho) = \alpha\beta\big(\beta^2-\alpha^2\big)\frac{1}{\beta\coth\alpha\rho - \alpha\coth\beta\rho} \tag{28}$$

$$\chi_o(\rho) = \alpha\beta\big(\beta^2-\alpha^2\big)\frac{1}{\beta\tanh\alpha\rho - \alpha\tanh\beta\rho}. \tag{29}$$

In typical microdrop experiments (Gaur and Miller, 1989, Jakubowski, 1990), the background fiber stress (σ_f) is much less than the fiber stress required to break the fiber/matrix bond ($-\sigma_m V_2/V_1$). When this situation holds, all terms involving σ_f are negligible and we can simplify the analysis by assuming that $\sigma_f = \sigma_0 = 0$. The total strain energy reduces to

$$U = 2C_{55}\rho\pi r_1^3 \left[\frac{D_3^2 \Delta T^2}{C_{33}^2} \left(\frac{C_{33}}{C_{55}} - \frac{\chi_e(\rho)}{\rho} \right) + \left(\frac{\sigma_m V_2}{2V_1} \right)^2 \left(\frac{\chi_e(\rho) + \chi_o(\rho)}{\rho} \right) \right]. \tag{30}$$

Because variational mechanics specifically minimizes energy, we expect eqn (30) to give a good approximation to the total microdrop strain energy. With unusual geometries for which the basic assumptions are invalid, however, the approximate strain energy can give poor results. The main problem is as ρ gets small. In the limit as ρ approaches zero, $\chi_o(\rho)$ approaches ∞ which causes the strain energy to diverge. By investigating microdrops of different sizes, we concluded that eqn (30) is valid as long as the microdrop is longer than it is wide; i.e. as long as $l \geq 2r_1$. In terms of dimensionless quantities, this requirement translates to $\rho \geq 1/\sqrt{V_1}$. In the next section we quote some typical experimental results where $V_1 = 5\%$ (Jakubowski, 1990) and thus we require $\rho \geq 4.5$. Fortunately, experimental microdrops are always longer than this required minimum length and we therefore expect eqn (30) to be a good approximation for all real microdrops.

SAMPLE STRESS STATE

A microdrop debond experiment begins with a fiber and microdrop under little or no load ($\sigma_f = 0$ or σ_f small). The knife edges are placed near the microdrop and the fiber is pulled. The pulling will put compressive stress on the matrix and the magnitude of σ_m will increase as the fiber is pulled. For a sample calculation we pick a low value of σ_f ($\sigma_f = 10$ MPa) and set σ_m to -100 MPa. To include thermal stresses we pick a typical ΔT of -125°C. Lastly, we pick fiber volume fraction and microdrop length. Typical experimental results have $V_1 = 5\%$ and length = 10 fiber diameters or about 80 μm when using graphite fibers (Jakubowski, 1990). The fiber and matrix properties used are listed in the Appendix. The far-field axial fiber stress for $\sigma_0 = V_1\sigma_f = 0.5$ MPa and $\Delta T = -125$°C is $\psi_0 = -300$ MPa. The far-field fiber stress is compressive due to axial thermal shrinkage of the microdrop relative to the fiber. The far-field radial stress at the fiber/matrix interface is

$$\sigma_{rr,1}(1)\,(\text{far field}) = -\frac{\mathrm{V_2}}{\mathrm{V_1}} \left(\frac{\mathrm{A_3}\psi_0 + \mathrm{A_5}\sigma_0 + \mathrm{A_5}\Delta\mathrm{T}}{\mathrm{A_0}} \right) = -11.1 \text{ MPa}. \tag{31}$$

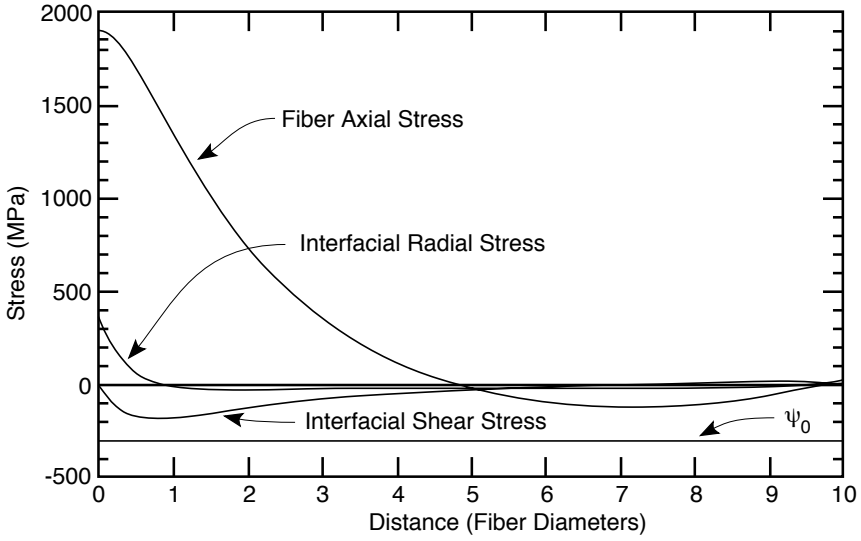

Fig. 3. The fiber axial stress, interfacial shear stress, and interfacial radial stress in a microdrop specimen. The horizontal line labeled ψ_0 is the far-field fiber axial stress. The distance axis is distance from the knife edges. The compressive stress applied to the matrix is -100 MPa; the background fiber stress is 10 MPa; the total microdrop length is 10 fiber diameters.

The far-field radial stress is compressive due to a shrink-fit of the matrix around the fiber caused by radial thermal contraction of the matrix.

The stresses that result from the assumed loading conditions in the previous paragraph are given in Fig. 3. The ordinate gives distance from the knife edges in units of fiber diameters. The axial fiber tensile stress at the knife edges is

$$\sigma_{zz,1}(\zeta = +\rho) = \sigma_f - \frac{V_2\sigma_m}{V_1} = 1910 \text{ MPa}. \tag{32}$$

At the opposite end of the microdrop the fiber stress is equal to the background stress, σ_f, or 10 MPa. Away from each end of the microdrop the fiber stress asymptotically approaches the far-field stress of $\psi_0 = -300$ MPa. A 10 fiber diameter microdrop with $V_1 = 5\%$ is short, however, and the fiber stress never gets close to ψ_0. Calculations with longer microdrops and the same V_1 show that the fiber stress reaches ψ_0 in 15-20 fiber diameters. In other words, for long microdrops (say 1000 fiber diameters) the fiber stress will be nearly equal to ψ_0 at positions more than 15-20 fiber diameters from either end. For microdrops with $V_1 \neq 5\%$, the distance required to reach ψ_0 decreases as V_1 increases.

The interfacial shear stress is zero on both ends of the microdrop as required by boundary conditions. Near the knife edges the shear stress peaks at −180 MPa and then returns towards zero. Near the opposite end of the microdrop there is a small peak in shear stress of 19.5 MPa. The form of the shear stresses differs significantly from that predicted by simplistic shear-lag models (Cox, 1952, Rosen, 1964, Amirbayat and Hearle, 1969, Kelly and Tyson, 1965). The simplistic models predict a maximum shear stress at the two ends of the microdrop. A peak shear stress at the microdrop ends, however, violates boundary conditions and results in an inadmissible stress state (Whitney and Drzal, 1987). We suggest that the variational mechanics analysis gives a more accurate description of the true interfacial shear stresses.

Near the knife edge, the interfacial radial stress is tensile and peaks at 366 MPa. The radial tensile stress concentration is caused, in part, by the matrix compressive stress and the resulting differential Poisson's contraction between the fiber and matrix (Broutman and McGarry, 1962). The radial stress decreases to a plateau value that is similar in magnitude but more compressive than the far-field radial compressive stress. If the microdrop was longer, the radial stress would be nearly equal to the far-field radial compressive stress at positions more than 15-20 fiber diameters from either end (for $V_1 \approx 5\%$). At the opposite end of the microdrop, the radial stress has a slight tensile stress concentration of 33 MPa. We note that simplistic, one-dimensional stress analyses (Cox, 1952, Rosen, 1964, Amirbayat and Hearle, 1969, Kelly and Tyson, 1965) do not determine the radial stress. Because the interfacial radial stress is tensile and is larger in magnitude that the interfacial shear stress, it probably plays a significant role in interfacial failure and therefore should not be ignored.

FAILURE ANALYSES

The goal of the microdrop debond test is to characterize the quality of the fiber/matrix interface. The experimental observable is the force required to dislodge the microdrop from the fiber; i.e. the force required to break the interface. Previous microdrop debond experiments used a simplistic analysis [e.g. shear lag (Cox, 1952, Rosen, 1964, Amirbayat and Hearle, 1969) or elastic-plastic (Kelly and Tyson, 1965) analyses] and calculated an interfacial shear strength or the critical interfacial shear stress, τ_{ic}, using

$$\tau_{ic} = \frac{F}{2\pi r_1 l}. \tag{33}$$

In eqn (33), F is the failure force above the background force and l is the length of the microdrop. In terms of the stresses used in this paper, eqn (33) becomes

$$\tau_{ic} = -\frac{1}{4\rho}\frac{\sigma_m V_2}{V_1}. \tag{34}$$

We let $\sigma_d = -\sigma_m V_2/V_1 = F/\pi r_1^2$ be the fiber stress above background at the force that causes the fiber and microdrop to debond. For a constant interfacial strength, eqn (33) predicts that σ_d will be proportional to ρ.

For a specimen that would fail under the stress example in Fig. 3, the interfacial shear strength would be $\tau_{ic} = 48$ MPa. This interfacial shear strength does not correspond to any obvious feature of the microdrop specimen stress state. To get a physical interpretation of τ_{ic} we express it in terms of $\psi(\zeta)$ as

$$\tau_{ic} = \frac{1}{4\rho}\big(\psi(\rho) - \psi(-\rho)\big) = \frac{r_1}{l}\int_{-\rho}^{\rho} \frac{\psi'(\zeta)}{2} d\zeta = \frac{1}{l}\int_{-l/2}^{l/2} \tau_{rz}(r_1, z)\, dz = \langle \tau_{rz}(r_1) \rangle\,. \tag{35}$$

In other words, the simplistic failure analysis equates the interfacial shear strength with the *average* interfacial shear stress along the length of the microdrop at the time of failure. Considering the complexity of the microdrop specimen stress state, it is unlikely that the average shear stress controls interfacial failure. Instead, fiber/matrix debonding should be expected to initiate at local stress concentrations and later propagate to cause complete debonding. Two interfacial stress concentrations are the tensile radial stress at the knife edges and the peak shear stress that occurs near the knife edges. The larger of these interfacial stresses is the radial stress. Because the peak radial stress is tensile, a likely failure mechanism is mode I or opening mode fracture initiating at the knife edges. If, as suggested, the peak force in the microdrop debond experiment corresponds to tensile failure of the interface, it is inappropriate to use eqn (33) and claim to be measuring an interfacial shear strength.

To appropriately analyze microdrop debonding experiments, it is essential to use a failure analysis that corresponds to the real interfacial failure process. Without extensive experimental results it is not possible to accept or reject any particular failure model, but, using the new variational stress analysis we can explore alternative failure criteria. Three potential failure criteria, all of which should be more realistic than the simple average shear stress approach, are:

(1) **Maximum Stress:** assume that interfacial failure occurs when some local interfacial stress reaches a critical value.
(2) **Total Energy:** assume that interfacial failure occurs when the total strain energy in the microdrop reaches a critical value.
(3) **Energy Release Rate:** assume that interfacial failure occurs when the energy release rate for initiation of a fiber/matrix debond at the knife edges exceeds a critical value.

The maximum stress model simply states that the microdrop will debond when either the maximum interfacial radial stress exceeds the interfacial tensile strength or the maximum interfacial shear stress exceeds the interfacial shear strength. The maximum interfacial radial stress occurs at $\zeta = \rho$. If the interface fails in tension, the variational stress state gives the interfacial tensile strength as $\sigma_{ic} = \sigma_{zz}\,(r_1, l/2)$ or

$$\sigma_{ic} = \frac{\psi''(\rho)}{16}\left(3 + \nu_m + \frac{2(1+\nu_m)\ln V_1}{V_2} - \frac{V_2 A_1}{V_1 A_0}\right) - \frac{V_2}{V_1}\left(\frac{A_3\psi(\rho) + A_4\sigma_0 + A_5\Delta T}{A_0}\right). \tag{36}$$

The maximum interfacial shear stress occurs near the knifes edges—typically less than one fiber diameter from the knife edges. If the interface fails in shear, the variational stress state gives the interfacial shear strength as

$$\tau_{ic} = \max\left(\frac{\psi'(\zeta)}{2}\right). \tag{37}$$

The maximum stress model is more reasonable than the average shear stress model, but it still has two limitations. First, predicting failure at the value of one component of the stress in a multiaxial stress state is probably an oversimplification. Second, it requires accurate determination of the maximum stress. The variational stress analysis is approximate and the approximations are most severe near the specimen ends. The inaccuracies near the specimen ends are due, in part, to the assumption of $\sigma_{zz,2}$ being independent of r, and, in part, to the idealization of the boundary conditions. Thus, while the variational analysis accurately represents the overall stress and strain energy in a microdrop specimen, it should not be expected to provide quantitative predictions of specific maximum interfacial stresses. One thing that can be said in favor of the average shear stress approach is that eqn (33) can be derived from equilibrium arguments and therefore gives the exact average shear stress. The fact that it is one of the few exact relations available, however, is insufficient justification for using it to describe interfacial failure.

A major disadvantage of both the average shear stress and the maximum interfacial stress approaches is that they focus on a single stress component. In an attempt to account for all stress components we might try predicting interfacial failure when the total strain energy reaches a critical value—the total energy model. An advantage of this model is that we only require the variational analysis to provide total strain energy, which, as discussed above, is the most accurate feature of the analysis. Dividing eqn (30) by total interfacial area ($A = 2\pi r_1 l = 4\rho\pi r_1^2$), the total energy per unit interfacial area is

$$G_i = \frac{C_{55} r_1}{2}\left[\frac{D_3^2 \Delta T^2}{C_{33}^2}\left(\frac{C_{33}}{C_{55}} - \frac{\chi_e(\rho)}{\rho}\right) + \left(\frac{\sigma_m V_2}{2V_1}\right)^2 \left(\frac{\chi_e(\rho) + \chi_o(\rho)}{\rho}\right)\right]. \tag{38}$$

The total energy model predicts that the fiber and matrix will debond when G_i reaches the interfacial toughness or critical energy release rate G_{ic}. Solving eqn (38) for the fiber stress to cause debonding gives

$$\sigma_d = 2\sqrt{\frac{\frac{2\rho G_{ic}}{r_1 C_{55}} - \frac{D_3^2 \Delta T^2}{C_{33}^2}\left(\frac{\rho C_{33}}{C_{55}} - \chi_e(\rho)\right)}{\chi_e(\rho) + \chi_o(\rho)}}. \tag{39}$$

In contrast to eqn (33), which predicts a linear relation between debond stress and microdrop length, eqn (39) is nonlinear in microdrop length. A simple limiting result is found for long microdrops. As ρ gets large, both $\chi_e(\rho)$ and $\chi_o(\rho)$ approach constants and eqn (39) predicts that σ_d is asymptotically proportional to $\sqrt{\rho}$. The value of ρ required to obtain this limiting result depends on the mechanical properties of the fiber and matrix and on the dimensions of the microdrop.

The third, and perhaps most sophisticated model, is to use fracture mechanics and assume that the interface will fail when the energy release rate for initiation of an interfacial crack at the knife edges, G_i, exceeds the interfacial toughness or critical interfacial energy release rate, G_{ic}. The first step of this model is to calculate G_i. The calculation involves finding the stresses in the presence of an interfacial crack as illustrated in Fig. 4. The originally intact microdrop specimen now has a crack of length a or dimensionless length 2δ where $\delta = a/2r_1$.

The stress analysis of the cracked specimen involves finding the stresses in region I, the region near the cracked interface, and the stresses in region II, the remainder of the microdrop. Because the radial stress is tensile before failure, the crack should open and result in stress free fracture surfaces. Stress-free fracture surfaces mean that the only possible stress state in region I which has σ_{zz} independent of r is simple uniaxial stress. From the boundary conditions at the top of region I, the stresses in the fiber are:

$$\sigma_{zz,1} = \frac{\sigma_0 - \sigma_m V_2}{V_1} \qquad \text{and} \qquad \tau_{rz,1} = \sigma_{rr,1} = \sigma_{\theta\theta,1} = 0 \tag{40}$$

and the stresses in the matrix are

$$\sigma_{zz,2} = \sigma_m \qquad \text{and} \qquad \tau_{rz,2} = \sigma_{rr,2} = \sigma_{\theta\theta,2} = 0. \tag{41}$$

The total strain energy in region I is

$$U_I = 2\delta\pi r_1^3 \left[\frac{1}{2E_A}\left(\frac{\sigma_0 - \sigma_m V_2}{V_1}\right)^2 + \frac{V_2 \sigma_m^2}{2V_1 E_m}\right]. \tag{42}$$

When σ_f is negligible, as in typical experiments,

$$U_I = 2\delta\pi r_1^3 \left[\frac{\sigma_m^2 V_2}{2V_1}\left(\frac{V_2}{V_1 E_A} + \frac{1}{E_m}\right)\right]. \tag{43}$$

At the top of region II, the boundary conditions are identical to the microdrop boundary conditions in eqn (13). In region II the stresses are thus the stresses that exist in a microdrop of dimensionless length $2(\rho - \delta)$. From eqn (30), the strain energy in region II when σ_f is negligible is

$$U_{II} = 2C_{55}(\rho - \delta)\pi r_1^3 \left[\frac{D_3^2 \Delta T^2}{C_{33}^2}\left(\frac{C_{33}}{C_{55}} - \frac{\chi_e(\rho - \delta)}{\rho - \delta}\right) + \left(\frac{\sigma_m V_2}{2V_1}\right)^2 \left(\frac{\chi_e(\rho - \delta) + \chi_o(\rho - \delta)}{\rho - \delta}\right)\right] \tag{44}$$

The total strain energy in the cracked microdrop specimen is $U = U_I + U_{II}$ or

$$U = 2\pi r_1^3 \left\{ \delta \left[\frac{\sigma_m^2 V_2}{2V_1} \left(\frac{V_2}{V_1 E_A} + \frac{1}{E_m} \right) \right] + (\rho - \delta) \frac{D_3^2 \Delta T^2}{C_{33}} \cdot \right.$$
$$\left. + C_{55} \left[\left(\left(\frac{\sigma_m V_2}{2V_1} \right)^2 - \frac{D_3^2 \Delta T^2}{C_{33}^2} \right) \chi_e(\rho - \delta) + \left(\frac{\sigma_m V_2}{2V_1} \right)^2 \chi_o(\rho - \delta) \right] \right\} \quad (45)$$

The total energy release rate associated with the growth of the fiber/matrix debond in Fig. 4 is

$$G_i = \frac{\partial W}{\partial A} - \frac{\partial U}{\partial A} \quad (46)$$

where W is external work, U is internal strain energy, and $A = 2\pi r_1 a = 4\pi r_1^2 \delta$ is total debond area. We consider the knife edges as fixed. When the debond extends at constant load, the only external work is the work done by the fiber stresses:

$$\frac{\partial W}{\partial A} = \frac{1}{4\pi r_1^2} \frac{\partial W}{\partial \delta} = \frac{1}{4} \left[\sigma_f \frac{\partial (u_f + u_d)}{\partial \delta} - \frac{\sigma_m V_2}{V_1} \frac{\partial (u_f - u_m)}{\partial \delta} \right] \quad (47)$$

where u_f, u_m, and u_d are the total debonded fiber displacement, debonded matrix displacement, and bonded microdrop displacement relative to the tip of the fiber/matrix debond (see Fig. 4). When

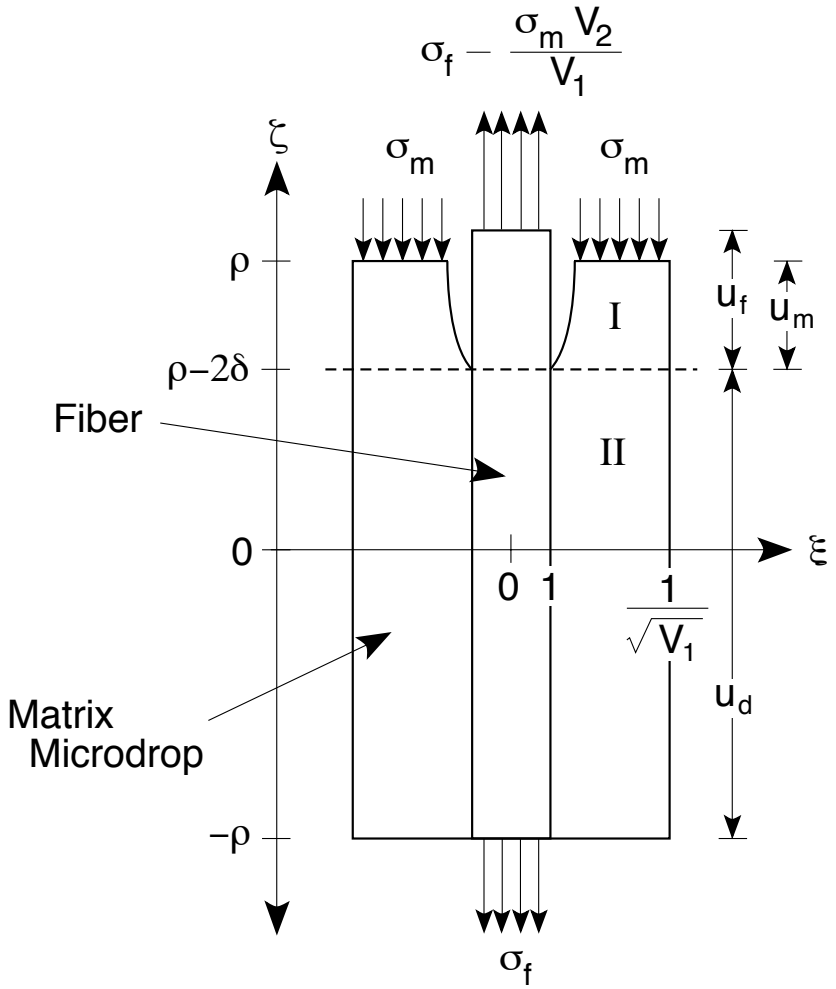

Fig. 4. An idealized matrix microdrop specimen of dimensionless length 2ρ having an interfacial crack of dimensionless length 2δ emanating for the top of the microdrop. Region I is the cracked region above the dashed line. Region II is the uncracked region below the dashed line.

σ_f is negligible we only need to consider the second term in eqn (47). By integrating the strains, the relevant displacement is

$$u_f - u_m = 2\delta r_1 \left[(\alpha_A - \alpha_m)\Delta T - \sigma_m \left(\frac{V_2}{V_1 E_A} + \frac{1}{E_m} \right) \right]. \tag{48}$$

Differentiating eqns (45) and (48), the final expression for energy release rate when σ_f is negligible is

$$\begin{aligned} G_i(\delta) &= \frac{r_1}{2} \Bigg\{ \frac{\sigma_m^2 V_2}{2V_1} \left(\frac{V_2}{V_1 E_A} + \frac{1}{E_m} \right) - \frac{\sigma_m V_2}{V_1} (\alpha_A - \alpha_m)\Delta T \\ &\quad + C_{55} \left[\frac{D_3^2 \Delta T^2}{C_{33}^2} \left(\chi_e'(0) - \chi_e'(\rho - \delta) \right) + \left(\frac{\sigma_m V_2}{2V_1} \right)^2 \left(\chi_e'(\rho - \delta) + \chi_o'(\rho - \delta) \right) \right] \Bigg\} \end{aligned} \tag{49}$$

The required derivatives are as follows. When $p^2 - 4q < 0$

$$\chi_e'(\rho) = 4\alpha\beta\left(\alpha^2 + \beta^2\right)^2 \frac{\sinh 2\alpha\rho \sin 2\beta\rho}{(\beta \sinh 2\alpha\rho + \alpha \sin 2\beta\rho)^2} \tag{50}$$

$$\chi_o'(\rho) = -4\alpha\beta\left(\alpha^2 + \beta^2\right)^2 \frac{\sinh 2\alpha\rho \sin 2\beta\rho}{(\beta \sinh 2\alpha\rho - \alpha \sin 2\beta\rho)^2}. \tag{51}$$

When $p^2 - 4q > 0$

$$\chi_e'(\rho) = \alpha^2\beta^2\left(\beta^2 - \alpha^2\right) \frac{\operatorname{csch}^2 \alpha\rho - \operatorname{csch}^2 \beta\rho}{(\beta \coth \alpha\rho - \alpha \coth \beta\rho)^2} \tag{52}$$

$$\chi_o'(\rho) = -\alpha^2\beta^2\left(\beta^2 - \alpha^2\right) \frac{\operatorname{sech}^2 \alpha\rho - \operatorname{sech}^2 \beta\rho}{(\beta \tanh \alpha\rho - \alpha \tanh \beta\rho)^2}. \tag{53}$$

In deriving eqn (49) we made use of the limiting relation

$$\lim_{\rho \to 0} \chi_e'(\rho) = \chi_e'(0) = \frac{C_{33}}{C_{55}}. \tag{54}$$

Because the strain energy in region II is only accurate for $\rho - \delta \geq 1/\sqrt{V_1}$, the energy release rate in eqn (49) is only valid for $0 \leq \delta \leq \rho - 1/\sqrt{V_1}$. Finally, an analogous energy release rate expression for $\sigma_f \neq 0$ can easily be derived, but the additional terms will normally be negligible.

By the energy release rate model, the fiber and matrix will debond when the energy release rate for initiation of a debond at the knife edges, $G_i(0)$, is equal to the fracture toughness of the interface, G_{ic}. From eqn (49), the stress to cause fiber and matrix debonding is predicted from the quadratic equation

$$\begin{aligned} &\sigma_d^2 \left[\frac{1}{2} \left(\frac{1}{E_A} + \frac{V_1}{V_2 E_m} \right) + \frac{C_{55}}{4} \left(\chi_e'(\rho) + \chi_o'(\rho) \right) \right] + \sigma_d (\alpha_A - \alpha_m)\Delta T \\ &\quad = \frac{2G_{ic}}{r_1} - C_{55} \frac{D_3^2 \Delta T^2}{C_{33}^3} \left(\chi_e'(0) - \chi_e'(\rho) \right). \end{aligned} \tag{55}$$

Equation (55) predicts a nonlinear relation between debonding stress and microdrop length. A new limiting result is found for long microdrops. As ρ gets large, both $\chi_e'(\rho)$ and $\chi_o'(\rho)$ approach zero and eqn (55) predicts that σ_d is asymptotically independent of ρ. The value of ρ required to obtain this limiting result depends on the mechanical properties of the fiber and matrix and on the dimensions of the microdrop.

CONCLUSION

We have described a variational mechanics analysis for the stresses and strain energy in microdrop debond specimens. The new stress analysis was used to develop several potential methods for analyzing microdrop debonding experimental results. All methods have one thing in common—each

predicts that the higher the debonding stress, the higher the interfacial strength or toughness. Thus, if your only goal is to rank interfaces in nominally identical specimens, any approach will suffice. In fact, measuring only the debonding stress without any attempt at reducing it to an interfacial strength or toughness will also suffice. If your goal, however, is to understand interfacial failure, if your goal is to compare results from different size specimens, or if your goal is to measure a physically valid interfacial strength or toughness that can be compared to other toughness results, it is essential to interpret microdrop debond results with a realistic model and an accurate stress analysis.

The three failure analysis models described in this paper can only be accepted or rejected by experimental studies. For example, the simple average shear stress model predicts that σ_d will be linear in ρ, while the total energy and energy release rate model predict that σ_d will asymptotically be proportional to $\sqrt{\rho}$ or be constant, respectively, as ρ gets large. Experiments over a sufficiently wide range of ρ, including large ρ, can determine which model, if any, is preferred. Although some have measured σ_d as a function of microdrop length(Jakubowski, 1990), the current range of data and the unfortunate scatter precludes us from determining which of our failure criteria is most accurate. We suggest that more extensive microdrop debond experiments are required. We further suggest that the scatter needs to be reduced. Two possible sources of scatter are real variations in the interfacial properties and experimental technique. If all the scatter is due to real variations in the interfacial properties than there is little hope of achieving a quantitative analysis of microdrop debond data. We can hope, however, that refinement of experimental technique will reduce the scatter. For example, we suggest replacing the knife-edge loading with axisymmetric loading. Axisymmetric loading might improve reproducibility and it at least more closely matches the boundary conditions of the variational stress analysis. Combining improved experimental technique with the improved failure analyses suggested in this paper can potentially result in a very useful microdrop debond method for characterizing the fiber-matrix interface.

Finally, we acknowledge the possibility that improved data may not fit any of our proposed failure analysis models. Such a negative result does not necessarily mean that we should reject the variational stress analysis and start over. More likely, we would only need to reject the failure criteria. Any new failure criteria that might seem appropriate can be developed into a microdrop failure model by using the variational stress analysis in this paper to predict the debonding stress.

Acknowledgments—This work was supported in part by a contract from NASA Langley Research Center (NAS1-18833) monitored by Dr. John Crews and in part by a gift from E. I. duPont deNemours & Company monitored by Dr. Alan R. Wedgewood. We also thank Dr. James Jakubowski of DOW Chemical for supplying typical experimental results.

REFERENCES

Amirbayat, J. and Hearle, W. S. (1969). Properties of unit composites as determined by the properties of the interface. Part I: Mechanism of matrix–fibre load transfer. *Fiber Sci. Tech.*, **2**, 123–141 (1969).

Bascom, W. D. and Jensen, R. M. (1986). Stress transfer in single fiber/resin tensile tests. *J. Adhesion*, **19**, 219–239 (1986).

Broutman, L. J. and McGarry, F. J. (1962). Glass–resin joint strength studies. *Modern Plastics*, **40**, 161–170 and 238–242 (1962).

Cox, H. L. (1952). The elasticity and strength of paper and other fibrous materials. *Brit. J. Appl. Phys.*, **3**, 72–79 (1952).

DiBenedetto, A. T. and Lex, P. J. (1989). Evaluation of surface treatments for glass fibers in composite materials. *Polymer Comp.*, **29**, 543–555 (1989).

DiLandro, L., DiBenedetto, A. T. and Groeger, J. (1988). The effect of fiber–matrix stress transfer on the strength of fiber–reinforced composite materials. *Polymer Comp.*, **9**, 209–221 (1988).

DiLandro, L. and Pegoraro, M. (1987). Carbon fiber–thermoplastic matrix adhesion. *J. Mater. Sci.*, **22**, 1980–1986 (1987).

Drzal, L. T., Rich, M. J., Camping, J. D. and Park, W. J. (1980) Interfacial shear strength and failure mechanisms in graphite fiber composites. *Proc. 35th Conf. of the SPI Reinforced Plastics Division*, Section 20-C, pp. 1–7.

Drzal, L. T., Rich, M. J. and Koenig, M. F. (1985). Adhesion of graphite fibers to epoxy matrices: III: The effect of hygrothermal exposure. *J. Adhesion*, **18**, 49–72 (1985).

Drzal, L. T., Rich M. J., Koenig, M. F. and Lloyd, P. F. (1983). Adhesion of graphite fibers to epoxy matrices: II. The effect of fiber finish. *J. Adhesion*, **16**, 133–152 (1983).

Drzal, L. T., Rich M. J. and Lloyd, P. F. (1982). Adhesion of graphite fibers to epoxy matrices: I. The role of fiber surface treatment. *J. Adhesion*, **16**, 1–30 (1982).

Folkes, M. J. and Wong, W. K. (1987). Determination of interfacial shear strength in fibre–reinforced thermoplastic composites. *Polymer*, **28**, 1309–1314 (1987).

Fraser, A. A., Ancker, F. H. and DiBenedetto, A. T. (1980) A computer modeled, single filament technique for measuring coupling and sizing agent effects in fiber reinforced composites. *Proc. 30th Conf. of the SPI Reinforced Plastics Division*, Section 22-A, pp. 1–13.

Fraser, W. A., Ancker, F. H., DiBenedetto, A. T. and Elbirli, B. (1983). Evaluation of surface treatments for fibers in composite materials. *Polymer Comp.*, **4**, 238–248 (1983).

Gaur, U. and Miller, B. (1989). Microbond method for determination of the shear strength of a fiber/resin interface: evaluation of experimental parameters. *Comp. Sci. Tech.*, **34**, 35–51 (1989).

Hashin, Z. (1985). Analysis of cracked laminates: a variational approach. *Mech. Mater.*, **4**, 121–136 (1985).

J. Jakubowski (1990). personal communication.

Kelly, A. and Tyson, W. R. (1965). Tensile properties of fibre-reinforced metals: copper/tungsten and copper/molybdenum. *J. Mech. Phys. Solids*, **13**, 329–350 (1965).

Mandell, J. F., Chen, E. J. H. and McGarry, F. J. (1980). A microdebonding test for *in situ* assessment of fiber/matrix bond strength in composite materials. *Int. J. Adhes.*, **1**, 40–44 (1980).

Nairn, J. A. (1992). A variational mechanics analysis of the stresses around breaks in embedded fibers. *Mech. Mater.*, **13**, 131–154 (1992).

Netravali, A. N., Schwartz, P. and Phoenix, S. L. (1989). Study of interfaces of high–performance glass fibers and DGEBA–based epoxy resins using single–fiber–composite test. *Polymer Comp.*, **10**, 385–388 (1989).

Ohsawa, T., Nakayama, A., Miwa, M. and Hesegawa, A. (1978). Temperature dependence of critical fiber length for glass fiber-reinforced thermosetting resins. *J. Appl. Polymer Sci.*, **22**, 3203–3212 (1978).

Penn, L. S., Bystry, F. A. and Marchionni, H. J. (1983). Relation of interfacial adhesion in Kevlar ®/epoxy systems to surface characterization and composite performance. *Polymer Comp.*, **4**, 26–31 (1983).

Piggott, M. R. (1987). Debonding and friction at fiber–polymer interfaces. I: Criteria for failure and sliding. *Comp. Sci. Tech.*, **30**, 295–306 (1987).

Piggott, M. R., Chua, P. S. and Andison, D. (1985). The interface between glass and carbon fibers and thermosetting polymers. *Polymer Comp.*, **6**, 242–248 (1985).

Rich, M. J. and Drzal, L. T. (1986) Interfacial properties of some high–strain carbon fibers in an epoxy matrix. *Proc. 41st Conf. of the SPI Reinforced Plastics Division*, Section 2-F, pp. 1–5.

Rosen, B. W. (1964) Mechanics of composite strengthening. In: *Fiber Composite Materials*, Chapter 3, pp. 37–75, American Society of Metals, Metals Park, Ohio.

Scheer, R. J. and Nairn, J. A. (1991). Variational mechanics analysis of the stresses in microdrop debond specimens. *Proc. 8th Int. Conf. on Composite Materials*, 29-C, 1–10.

Wadsworth, N. J. and Spilling, I. (1968). Load transfer from broken fibres in composite materials. *Brit. J. Appl. Phys. (J. Phys. D.)*, **1**, 1049–1058 (1968).

Whitney, J. M. and Drzal, L. T. (1987). Axisymmetric stress distribution around an isolated fiber fragment. In *Toughened Composites*, ASTM STP 937 (Edited by N. J. Johnston), pp. 179–196.

APPENDIX

In Nairn (1992), the complementary energy was expressed in terms of constants that depend on the sample dimensions and on the mechanical properties of the fiber and the matrix:

$$A_0 = \frac{V_2(1-\nu_T)}{V_1 E_T} + \frac{1-\nu_m}{E_m} + \frac{1+\nu_m}{V_1 E_m} \tag{A1}$$

$$A_1 = \left(\frac{1-\nu_T}{E_T} - \frac{1-\nu_m}{E_m}\right)(1+\nu_m)\left(1+\frac{2\ln V_1}{V_2}\right) + \frac{2(1-\nu_m)}{V_2 E_m} \tag{A2}$$

$$A_2 = \frac{1-\nu_T}{E_T} - \frac{1-\nu_m}{E_m} \tag{A3}$$

$$A_3 = -\left(\frac{\nu_A}{E_A} + \frac{V_1\nu_m}{V_2 E_m}\right) \tag{A4}$$

$$A_4 = \frac{\nu_m}{V_2 E_m} \tag{A5}$$

$$A_5 = \alpha_T - \alpha_m \tag{A6}$$

$$C_{33} = \frac{1}{2}\left(\frac{1}{E_A} + \frac{V_1}{V_2 E_m}\right) - \frac{V_2 A_3^2}{V_1 A_0} \tag{A7}$$

$$C_{35} = \frac{1}{16}\left[A_3\left[(1+\nu_m)\left(1+\frac{2\ln V_1}{V_2}\right)-\frac{V_2A_1}{V_1A_0}\right]-2A_4\right] \tag{A8}$$

$$C_{55} = \frac{1}{256}\left\{\frac{1-\nu_T}{E_T}\left[\frac{5+2\nu_T}{3}+\nu_m(2+\nu_m)\right]+\frac{4A_2(1+\nu_m)^2\ln V_1}{V_2}\left(1+\frac{\ln V_1}{V_2}\right)-\frac{V_2A_1^2}{V_1A_0}\right.$$
$$\left.+\frac{1-\nu_m}{E_m}\left[\frac{V_2^2(1+\nu_m)(5+3\nu_m)-3V_2(1+\nu_m)(3+\nu_m)+6(5+3\nu_m)}{3V_1V_2}+\frac{8(1+\nu_m)\ln V_1}{V_2^2}\right]\right\} \tag{A9}$$

$$C_{44} = \frac{1}{16}\left[\frac{1}{G_A}-\frac{1}{G_m}\left(1+\frac{2}{V_2}+\frac{2\ln V_1}{V_2^2}\right)\right] \tag{A10}$$

$$C_{13} = -\frac{1}{2V_2E_m}-\frac{V_2A_3A_4}{V_1A_0} \tag{A11}$$

$$C_{11} = \frac{1}{2V_1V_2E_m}-\frac{V_2A_4^2}{V_1A_0} \tag{A12}$$

$$D_3 = -\frac{V_2A_3}{V_1A_0}\left[\alpha_T-\alpha_m\right]+\frac{1}{2}\left[\alpha_A-\alpha_m\right]. \tag{A13}$$

In these equations, E_A and E_T are the axial and transverse tensile moduli of the fiber, G_A is the axial shear modulus of the fiber, ν_A and ν_T are the axial and transverse Poisson's ratios of the fiber, α_A and α_T are the axial and transverse thermal expansion coefficients of the fiber, and E_m, G_m, ν_m, and α_m are the tensile modulus, shear modulus, Poisson's ratio, and thermal expansion coefficient of the matrix. The constants in eqns (9) and (12) are:

$$p = \frac{2C_{35}-C_{44}}{C_{55}} \qquad \text{and} \qquad q = \frac{C_{33}}{C_{55}} \tag{A14}$$

The sample stress state calculated in this paper is for a typical epoxy microdrop on a graphite fiber. We assumed the following properties for the fiber and matrix:

$$\begin{aligned} E_A &= 220000 \text{ MPa} & \qquad E_m &= 4300 \text{ MPa} \\ E_T &= 14000 \text{ MPa} & G_m &= \tfrac{E_m}{2(1+\nu_m)} = 1604 \text{ MPa} \\ G_A &= 35000 \text{ MPa} & \nu_m &= 0.34 \\ \nu_A &= 0.20 & \alpha_m &= 40.0\times10^{-6}\ \text{C}^{-1} \\ \nu_T &= 0.35 & & \\ \alpha_A &= -0.36\times10^{-6}\ \text{C}^{-1} & & \\ \alpha_T &= 18.0\times10^{-6}\ \text{C}^{-1}. & & \end{aligned} \tag{A15}$$